ELSEVIER

Journal of Nuclear Materials 266–269 (1999) 877–883

journal of nuclear materials

Edge localised asymmetric radiative phenomena in RFX

L. Marrelli [a,*], P. Zanca [a], P. Martin [a,b], S. Martini [a], A. Murari [a]

[a] *Consorzio RFX, Corso Stati Uniti, 4 35127 Padova, Italy*

[b] *Physics Department, University of Padova and Istituto Nazionale di Fisica della Materia, UdR Padova, Italy*

Abstract

Measurements performed with a high resolution tomography system have shown that the total radiation patterns in the RFX plasmas are characterised by remarkable structures, localised in the edge and asymmetric, both in the toroidal and in the poloidal directions. The main source of symmetry breaking in the toroidal direction is mode locking i.e. unstable MHD modes lock in phase and to the wall during the setting-up of the magnetic configuration and produce a toroidally localised macroscopic distortion of the plasma surface with enhanced plasma wall interaction. In this paper the toroidal and poloidal structure of the stationary emissivity profiles in the locked mode region will be presented and its correlation with the local position and shape of the magnetic perturbation will be highlighted, thus giving a more complete picture of the locked mode structure in particular at the plasma edge.

Keywords: Edge radiation; Emission asymmetry; Radiation loss; RFX; Reversed field pinch

1. Introduction

The RFX device [1] (major radius $R = 2$ m, minor radius $a = 0.46$ m, plasma current $I_p \leqslant 2$ mA) is presently the largest Reversed Field Pinch (RFP) in operation. The RFP is a high magnetic shear configuration which is almost entirely produced by internal plasma currents parallel to the magnetic field. This entails a 'dynamo' mechanism which is driven by a spectrum of global tearing modes resonant inside the field reversal surface [2]. The dynamo modes are typically phase-locked between themselves and, with a few exceptions, in RFX are also locked to the wall, so that all pulses exhibit large magnetic deformations (in the following referred to as locked modes, LM) [3,4]. The macroscopic effect of the locked modes is a perturbation of the equilibrium magnetic field which causes an helical distortion of the plasma column. This determines, in a region extending 30°–50° toroidally, a helical displacement of the plasma column of about 1–3 cm from the axisymmetric position [2]. The toroidal location of the perturbed region is determined at the beginning of the RFP phase and generally remains approximately stationary through most of the discharge [3,5]. On the other hand, the LM position is influenced both by distributed field errors, such as toroidal field ripple, and by local field errors, as those due to the poloidal field gaps, pumping ducts and diagnostic holes in the stabilising conducting shell. The LM position then usually varies randomly from shot to shot: this peculiarity of the LM allows for a statistical characterisation of the perturbed region.

LM induced distortions, as in other RFP experiments [6], cause severe plasma–wall interactions [7,8]. Heat fluxes as high as 200 MW/m^2 have in fact been measured in the region interested by mode locking and they can cause heating of plasma facing components up to the sublimation temperature.

Despite the significant improvement in the comprehension of locked modes phenomenology in RFX, the role of the induced perturbation on the global power balance is still an open question. In particular, radiation losses in the perturbed region were only indirectly estimated [8], and no information about their spatial distribution was available up to now. In order to address such issue, an experimental campaign of 106 similar

* Corresponding author. Tel.: +39 49 829 5006; fax: +39 49 870 0718; e-mail: marrelli@igi.pd.cnr.it.

0022-3115/99/$ – see front matter
PII: S0022-3115(98)00554-6

discharges with plasma current $I_p \approx 0.55$–0.65 mA, and electron density n_e between 1 and 5×10^{19} m^{-3} has been conducted. This paper presents a detailed survey of the LM induced radiative phenomenology, paying particular attention to the plasma surface interaction, and correlates it to the magnetic structure of the perturbation. The analysis has been carried out by integrating the measurements performed with a high resolution tomographic system with the results of a recently developed magnetic reconstruction code.

The paper is organised as follows. In Section 2 some details concerning the RFX bolometric tomography and the reconstruction technique are given. Section 3 deals with the results of the magnetic equilibrium code, whereas in Section 4 the structure of total radiation emissivity profile is described. Conclusions are drawn in Section 5.

2. Bolometric tomography

Among the various diagnostic systems which equip RFX [9] the bolometric tomography is one of the most complex [10]. The bolometric detectors which have been used are the same adopted in the major tokamaks [11]. In this work, to reconstruct the bolometric emissivity a maximum entropy constrained finite element approach [12–15] has been considered. This choice has been suggested by the geometry of lines of sight, arranged in three overlapping fans of 12 lines-of-sight each, which cover the plasma poloidal cross section in a nonhomogeneous way, resulting in a nonuniform spatial resolution.

The emissivity is supposed to be constant over plasma regions ('pixels') of suitably chosen shape: in our case the pixels in the *plasma core* are simple concentric rings, of radial extent equal to 10% of the minor plasma radius (approximately corresponding to the average distance between adjacent lines of sight). The assumption of poloidal symmetry in the plasma core is motivated by the strong parallel transport along magnetic surfaces and by the absence of impurity sources in the core. In the *edge region*, defined as the outer 30% of plasma minor radius, the annular rings are divided in poloidal sectors since poloidal asymmetries are expected due to localised interaction between the plasma and the first wall.

3. Reconstruction of the plasma surface

3.1. Technique

In RFX the plasma surface (defined as the magnetic surface where the current density vanishes) is reconstructed by various programs which use the magnetic measurement provided by a system of probes [16], located on the inner surface of the conducting stabilising shell and arranged in toroidal and poloidal arrays. The programs solve the vacuum Maxwell equations in the region comprised between the vacuum vessel and the shell.

The detailed shape of the plasma surface can be determined only at the toroidal angles $\phi = 87°$ and $\phi = 207°$, where two poloidal arrays consisting of 16 radial and poloidal field probes are located. When the LM perturbation is far away from $\phi = 87°$ and $\phi = 207°$ the results are in good agreement with the standard equilibrium theory, i.e. a plasma with a circular cross section of radius $\approx a$ (the elongation and the triangularity are almost negligible) and with an horizontal shift given by the Shafranov formula [17]. On the other hand, by analysing discharges where LM perturbation is close to the measuring positions, the local horizontal and vertical shift of the plasma surface result strongly perturbed (about 1–3 cm from the average value), while the elongation and the triangularity are left nearly unchanged. The overall picture is consistent with a LM perturbation made of a superposition of $m = 1$ modes [3].

To obtain an estimate of the plasma shift at each toroidal position, the measurement of two toroidal arrays of 72 toroidal field probes can be used; this is useful to correlate the perturbation of the total radiation emissivity (measured by the tomographic diagnostic at $\phi = 202.5°$), induced by the LM, with the plasma surface distortion. In principle, it is not possible to determine the local shift with only one field component, since the solution of the Maxwell equations requires both a field parallel to the shell (either B_ϕ or B_θ) and the radial field B_r, which describes the penetration of the shell by the magnetic surfaces. Nevertheless, a statistical analysis of the local shape of the plasma surface at $\phi = 87°$ and $\phi = 207°$ shows that, in the time interval 40–60 ms (i.e. during the flat top phase of the discharge), the penetration of the shell by the magnetic perturbation is such that the B_r contribution is nearly equivalent to that of the toroidal component B_ϕ, so that the following approximate formula can be adopted:

$$\Delta B_\phi(\phi,\theta) = \frac{\mu_0 I_p}{2\pi b}\frac{1}{R}\left[\cos\theta\frac{d}{d\phi}\Delta V(\phi) - \sin\theta\frac{d}{d\phi}\Delta H(\phi)\right], \tag{1}$$

where $\Delta B_\phi(\phi,\theta)$ is the toroidal field perturbation at the shell, $\Delta H(\phi)$, $\Delta V(\phi)$ are the horizontal and vertical shifts, $b = 0.538$ m is the shell radius and I_p is the plasma current. Eq. (1) gives a complete description of the distortion of the plasma column caused by the locked modes: for any toroidal angle ϕ it gives the amplitude of the displacement $|\Delta(\phi)|$ from the equilibrium position and its poloidal direction $\theta(\phi) = \mathrm{arctg}(\Delta V(\phi)/\Delta H(\phi))$.

3.2. Results

In Fig. 1 the typical shape of the perturbation is shown (solid line). The toroidal angle in which the function $|\Delta(\phi)|$ reaches the maximum value will be called the locking angle (ϕ_{lock}) and will be used in the following to identify the position of the locked mode. It is worth noting that the data points, representing $|\Delta(\phi = 202.5°)|$ for all of the shots of the campaign plotted vs. ϕ_{lock}, are fitted very well by the typical profile: therefore the toroidal profile of the magnetic perturbation can be considered similar for all discharges considered here.

An important point to raise is that for this set of discharges the [ϕ_{lock}, $\theta(\phi_{\text{lock}})$] couples are not evenly distributed over the toroidal surface which enclose the plasma. In the toroidal region in proximity of the tomographic diagnostic cross section, [ϕ_{lock}, $\theta(\phi_{\text{lock}})$] tends to be concentrated along an helical path, with poloidal and toroidal mode numbers equal to $m = 1$ and $n \approx 8$, respectively, whose pitch approximately corresponds to the typical one of the magnetic perturbation of a single discharge (see Fig. 2). This implies that, for this set of discharges, the perturbation of the plasma surface position at the tomographic diagnostic cross section is always directed toward the inner region of the plasma wall, that is $90° < \theta(\phi = 202.5°) < 180°$, where the 0° direction of the polar co-ordinate system (see Fig. 3) lays in the equatorial plane and points toward

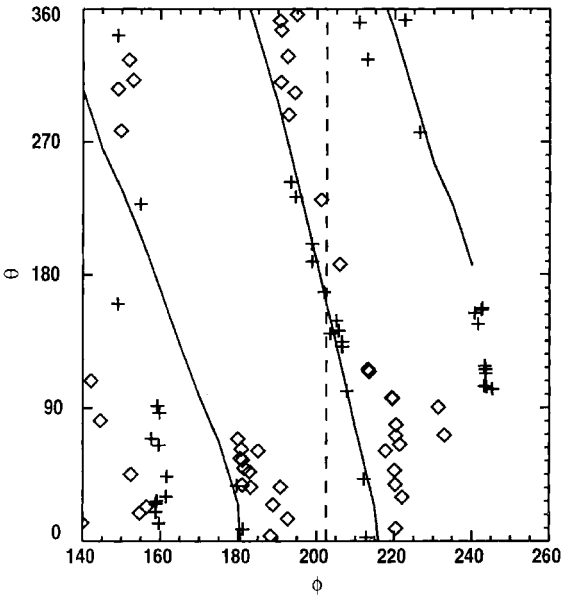

Fig. 2. Poloidal $\theta(\phi_{\text{lock}})$ and toroidal ϕ_{lock} location of the magnetic perturbation maxima over the toroidal surface enclosing the plasma. Diamonds represent discharges whose poloidal direction of the magnetic perturbation at the tomographic diagnostic is $180° < \theta(\phi = 202.5°) < 360°$, while crosses $0° < \theta(\phi = 202.5°) < 180°$. The continuous line represents the poloidal direction $\theta(\phi)$ of the plasma position perturbation for an individual shot.

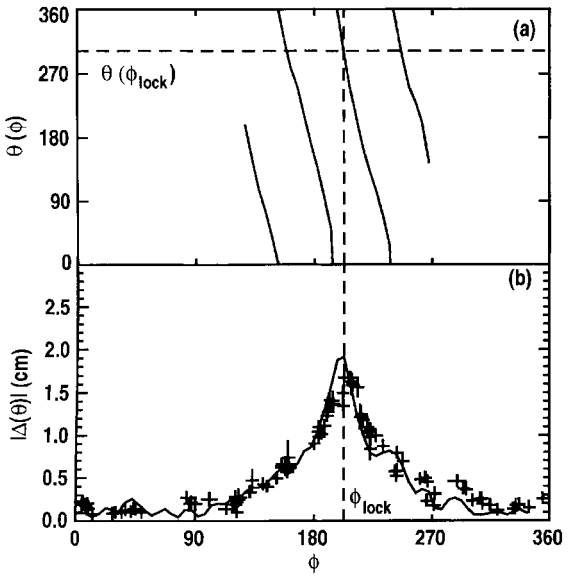

Fig. 1. Typical shape of the magnetic perturbation, when locked at $\phi = 202.5°$ (a) Poloidal direction of the perturbation of plasma position $\theta(\phi)$ at any toroidal position. (b) Amplitude of $|\Delta(\phi)|$ of the plasma position perturbation (continuous line). The locking angle ϕ_{lock}, defined as the angle at which total displacement reaches its maximum, is represented by the vertical dashed line. The poloidal direction of the displacement at the locking angle $\theta(\phi_{\text{lock}})$ is marked by the horizontal dashed line. Crosses represents the amplitude of perturbation as measured at $\phi = 202.5°$ plotted vs. the position ϕ_{lock} for the discharges considered in the paper.

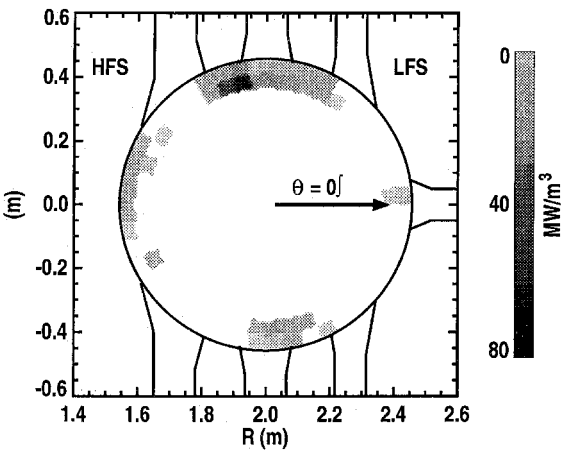

Fig. 3. Emissivity reconstruction for shot 6951. A significant enhancement in the upper region ($\theta = 90°$) near the central porthole may be observed.

the Low Field Side. Such behaviour has been observed in other toroidal locations and seems to be related to details concerning the field errors in RFX, since such pattern changes as the direction of the on axis toroidal field with respect to the plasma current is reversed.

4. Total radiation emissivity

4.1. Toroidally symmetric losses

A general property of unperturbed total radiation emissivity profiles in stationary conditions is that they are typically edge-peaked [18]: 80% of the radiated power P_{rad} comes from an outer layer of width 0.15–0.3a. In standard conditions P_{rad} accounts for approximately 10% of the input power P_{inp}, with the ratio increasing up to 40% in high density regimes.

RFX emissivity profiles are typically poloidally asymmetric. Such asymmetry is well correlated to the axisymmetric horizontal magnetic shift Δ_h [19,20] and with impurity influxes [21] (mainly carbon and oxygen in RFX, as the first wall is entirely covered by graphite). The enhancement of the emissivity can then be related to the increased interaction with the wall suffered by the plasma when its equilibrium is displaced.

4.2. Emissivity toroidal perturbation

The helical shaped region where the first wall of graphite is intersected by the distorted magnetic surfaces is interested by enhanced plasma wall interaction, which cause a dramatic increase of localised impurity influxes [8]. In this region, the spatial distribution of the total radiation emissivity is rather complex. While in some cases the emissivity is not significantly affected by the presence of locked modes, in other cases one or more poloidally localised, highly emitting regions suddenly appear at the plasma edge (see Fig. 3.). Very often these small regions, which may be characterised by large time fluctuations of the emissivity, are close to the edges of the graphite tiles.

A more quantitative picture emerges by studying the toroidal profile of the horizontal component of the emissivity 'centre of mass' x_g:

$$x_g = \int d\vartheta\, dr\, r_2\, \cos\vartheta\, \varepsilon(r,\vartheta) / \int d\vartheta\, dr\, r\varepsilon(r,\vartheta). \qquad (2)$$

The statistical dependence of x_g on $\phi_d = \phi_{lock} - 202.5°$, i.e. on the toroidal distance between the LM maximum and the bolometric tomography, is shown in Fig. 4.

First, it may be noticed that the maximum of x_g alteration occurs at $\phi_d = 0°$, that is exactly at the same toroidal location of the magnetic perturbation. Secondly, the emissivity centre of mass differs from the

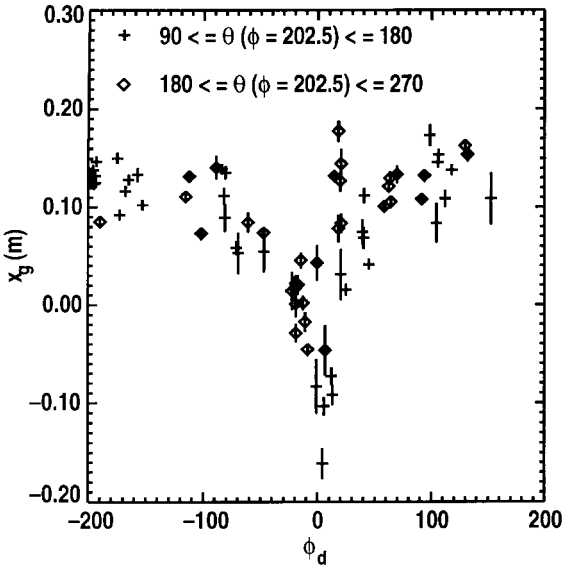

Fig. 4. Dependence of the horizontal component of the emissivity centre of mass x_g, on the toroidal angular distance from the maximum ϕ_d of the magnetic perturbation.

axisymmetric one in a toroidal region extending from −80° to 60°, whose width approximately corresponds to that of the magnetic perturbation (see Fig. 1).

As observed in the previous section, all of the discharges in the dataset considered in this paper are characterised by $90° < \theta(\phi_d) < 270°$, so that a complete characterisation of the poloidal dependence of the emissivity distribution is not possible, as no information about radiation losses is available where the local perturbation points toward the High Field Side.

Nevertheless, some interesting features emerges from Fig. 4, where the discharges have been classified according to the poloidal direction $\theta(\phi_d)$ of the local perturbation of plasma position. At a fixed ϕ_d value, i.e. at a fixed toroidal distance from the maximum, $x_g(\phi_d)$ is more perturbed when $90° < \theta(\phi_d) < 180°$ compared to discharges whose local perturbation is in the range $180° < \theta(\phi_d) < 270°$: the horizontal perturbation of the centre of mass is larger when the plasma surface is displaced upwards at the bolometric tomography toroidal location. This implies a poloidal dependence of $x_g(\phi_d)$ on $\theta(\phi_d)$, for fixed values of ϕ_d, as shown in Fig. 5: as $\theta(\phi_d)$ approaches 270°, $x_g(\phi_d)$ is similar to the average unperturbed centre of mass (which varies in the shaded region of the figure). The perturbation of the centre of mass grows when $\theta(\phi_d)$ decreases (i.e. when the local magnetic perturbation points toward the HFS) and reaches its maximum at $150° < \theta(\phi_d) < 180°$.

Such behaviour can be explained as the superposition of two different edge radiating regions. The first one is the toroidally symmetric annular layer described in the

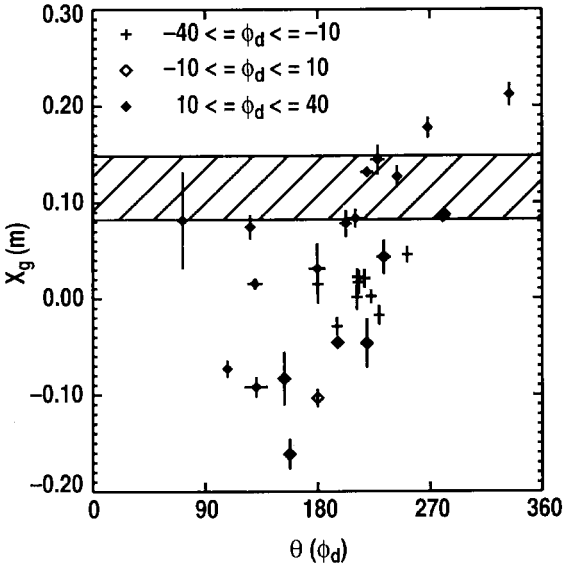

Fig. 5. Dependence of the horizontal component of the emissivity centre of mass x_g on the poloidal direction of the local displacement $\theta(\phi_d)$. Discharges have been grouped according to the toroidal distance from the maximum of the magnetic perturbation.

previous section. Since for the discharges analysed in this paper Δ_h was positive, in the range 1–1.5 cm, this originates an edge radiating layer with a stronger emission from the LFS. The second one, which is toroidally localised and due to the LM, is located in edge region in proximity of $\theta(\phi_d)$. When $\theta(\phi_d)$ approaches 270°, the first region emissivity dominates, and x_g is globally not perturbed. As soon as magnetic perturbation $\theta(\phi_d)$ points toward 180°, the first region emissivity gets weaker since the plasma column is locally more centred, and the second region becomes dominant: therefore, x_g is maximally affected when $\theta(\phi_d)$ is between 150° and 180°.

The poloidal direction $\theta(\phi_d)$ of the local perturbation of plasma position is not the only factor influencing bolometric losses in the perturbed region. In fact, for the same local displacement $\theta(\phi_d)$ of the plasma column, x_g seems to be more perturbed when $\phi_d > 0$ (Fig. 5). The interpretation of the latter evidence is still an open question, as several explanations may be given. First of all, the magnetic perturbations may slightly differ according to their toroidal location ϕ_{lock}. Moreover, the effect of the magnetic perturbation on radiation losses may depend on the toroidal ϕ_{lock} and poloidal $\theta(\phi_{lock})$ location of its maximum, due to structural details of RFX, as for example misalignment of the tiles on the first wall or field errors. Therefore, the distinction between data points in Fig. 5 may not be due to an intrinsic asymmetry between the regions preceding and following the maximum, but rather suggests that the perturbation of bolometric emissivity differs from shot to shot depending on $\theta(\phi_{lock})$: in fact, due to the aforementioned concentration of magnetic perturbations maxima along an helical path (Fig. 2), the $\phi_d > 0$ discharges are characterised by $\theta(\phi_{lock}) < 180°$, while for the $\phi_d < 0$ discharges $\theta(\phi_{lock})$ points toward the opposite direction.

The latter conclusion is strengthened as total radiation losses are considered (Fig. 6). In fact, the radiated power linear density Π_{rad}, defined as

$$\Pi_{rad} = \int d\vartheta \, dr \, r\varepsilon(r, \vartheta), \tag{3}$$

differs from its unperturbed value in a toroidal region narrower than that of the magnetic perturbation, and exhibits two different behaviours, depending on the poloidal direction of the local perturbation of plasma position $\theta(\phi_d)$. When $180° < \theta(\phi_d) < 270°$ no significant change of Π_{rad} is observed, while when $90° < \theta(\phi_d) < 180°$ a consistent increase, not constant in time during the discharge, is seen.

The results of Fig. 6 can be used to estimate the radiated power due to the locked modes induced plasma-wall interaction, for the two set of discharges mentioned above. Total radiation losses may be written as follows:

$$P_{rad} = \int d\Phi \, R\Pi_{rad}(\Phi), \tag{4}$$

where $\Pi_{rad}(\phi_d) = \Pi_{rad,sym} + \Pi_{rad,lock}(\phi_d)$, and $\Pi_{rad,sym}$ represents the axisymmetric component.

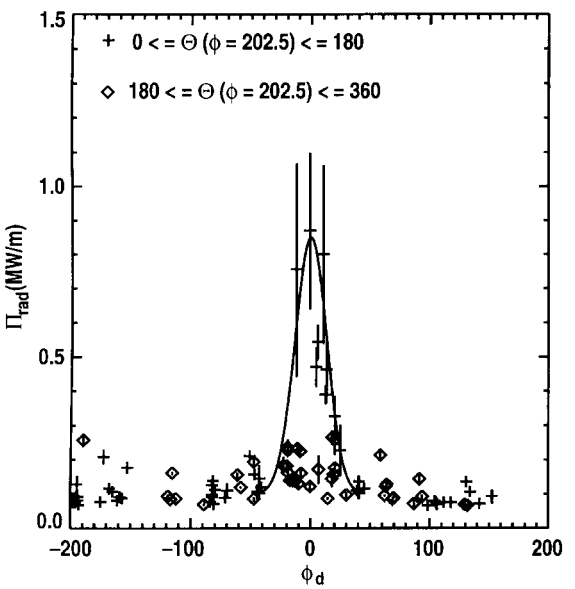

Fig. 6. Total radiated power linear density plotted vs. the toroidal angular distance ϕ_d from the maximum of the magnetic perturbation.

For highly radiating discharges $\Pi_{\mathrm{rad,lock}}(\phi_{\mathrm{d}})$ is a function sharply peaked around 0° and is approximately Gaussian-like

$$\Pi_{\mathrm{rad,\ lock}}(\phi_{\mathrm{d}}) = \Pi_0 \exp\left(-(\phi_{\mathrm{d}}/\sigma_{\Pi})\right), \tag{5}$$

where $\Pi_0 = 0.75$ MW/m and $\sigma_{\Pi} \approx 20°$. For the other discharges $\Pi_{\mathrm{rad,lock}}(\phi_{\mathrm{d}})$ is negligible. As a consequence, the LM induced bolometric loss term $P_{\mathrm{rad,lock}}$ is approximately 0.9 MW for highly radiating discharges, while it is negligible in the other cases.

As the unperturbed total radiated power linear density $\Pi_{\mathrm{rad,sym}}$ ranges between 0.07 and 0.15 MW/m, axisymmetric losses $P_{\mathrm{rad,sym}} = 2\pi R\ \Pi_{\mathrm{rad,sym}}$ varies between 0.7 and 1.5 MW, for this set of discharges.

The effect of LM induced magnetic perturbation on total radiation losses is therefore radically different, depending on $\theta(\phi_{\mathrm{lock}})$; when $180° < \theta(\phi_{\mathrm{lock}}) < 270°$ the localised contribution to bolometric losses is negligible while when $90° < \theta(\phi_{\mathrm{lock}}) < 180°$ the toroidally localised bolometric losses, in the highest cases, may be comparable to the axisymmetric ones. For this set of discharges, total radiation losses (toroidally localised and axisymmetric) account for up to 6–10% of total input power (which varied in the range 20–24 MW).

5. Conclusions

With the results presented in this paper we propose a more complete picture of the structure of the LM induced perturbation in RFX, in particular as far as plasma-wall interaction and radiative phenomena are concerned.

The perturbation of the equilibrium magnetic field due to LM has been studied in detail with the aid of dedicated magnetic reconstruction code. The LM-driven magnetic distortion causes a significant localised modification of the total radiation emissivity profile. Its pattern is somewhat more complicated than that of the magnetic perturbation, since it is influenced by the location of impurity sources and their transport along and across the perturbed magnetic field.

Nevertheless, given the localisation of the emissivity perturbation in a relatively narrow toroidal region, radiation losses in RFX do not seem to be severely influenced by the presence of LM, as the influence on the average global radiation losses is not in general very large.

These measurements then offer an independent confirmation that transport remains the major energy loss term and that it is just the transport channel which is most strongly affected by the presence of locked modes.

Spatial details of radiation losses have been studied quantitatively and correlated with both the toroidal and the poloidal location of the magnetic perturbation maximum. For the dataset considered in this paper, while the toroidal distribution of locked modes is somewhat uniform, it appears that each toroidal position has a preferred poloidal localisation of the maximum of the perturbation. This is probably dependent on RFX specific field errors pattern. Even if a complete statistical characterisation of the emissivity in the LM perturbed region was not possible, several interesting features emerge. In the toroidal direction, the locked modes perturbed region may be divided in three zones: the central one, spanning approximately 20° around the maximum, is characterised by a significant perturbation of the emissivity centre of mass and, in some cases, by a large and fluctuating enhancement of radiation. Two peripheric zones preceding and following the central one show only a perturbation of the emissivity and no appreciable change of the total radiated power level. Present data indicate that the emissivity behaviour in the peripheric zones is not symmetric about the magnetic perturbation maximum.

Both transport and radiation are affected when LM are present causing field lines to intercept the vessel. Nonetheless, while the perturbation of the energy transport mechanism affects the whole plasma and influences its global behaviour, the effect on the radiation losses remains local.

References

[1] G. Rostagni et al., Fus. Eng. Des. 25 (1995) 301.
[2] S. Ortolani, D.D. Schnack, Magnetohydrodynamics of Plasma Relaxation, World Scientific, Singapore, 1993.
[3] A. Buffa et al., 21st EPS conference on Plasma Physics and Controlled Nuclear Fusion, vol I, Montpellier, France, 1994, p. 458.
[4] V. Antoni et al., 22nd EPS Conference on Plasma Physics and Controlled Nuclear Fusion, vol. 4, Bournemouth, Great Britain, 1995, p. 181.
[5] T. Bolzonella et al., 23rd EPS Conference on Plasma Physics and Controlled Nuclear Fusion, vol. 2, Kiev, Ukraine, p. 633.
[6] A.F. Almagri, PhD thesis, University of Wisconsin–Madison, WI, 1990.
[7] T. Bolzonella et al., 22nd EPS Conference on Plasma Physics and Controlled Nuclear Fusion, vol. 4, Bournemouth, Great Britain, 1995, p. 177.
[8] M. Valisa et al., J. Nucl. Mater. 241–243 (1997) 988.
[9] M. Bagatin et al., Fus. Eng. Des. 25 (1995) 425.
[10] P. Martin et al., Rev. Sci. Instr. 68 (2) (1997) 1256.
[11] K.F. Mast, E.R. Müller, J. Appl. Phys. 55 (1984) 7.
[12] B. Buck (Ed.), Maximum Entropy in Action, Clarendon, Oxford, 1991, p. 109.
[13] T. Jaynes, Phys. Rev. 106 (1957) 620.
[14] T. Jaynes, Phys. Rev. 108 (1957) 171.
[15] S. Gull, G. Danniell, Nature 272 (1978) 686.
[16] A. Stella et al., Fus. Eng. and Des. 25 (1995) 373.

[17] V.D. Shafranov, Plasma equilibrium in a magnetic field, Reviews of Plasma Physics (Ed. Leontovich), vol.2 Consultants Bureau, New York, 1996, p. 103.
[18] A. Murari et al., Proceedings of the 23rd Conference on Controlled Fusion and Plasma Physics, vol. 20C part II, Kiev, Ukraine, 1996, p. 645.
[19] L. Marrelli et al., Nucl. Fus. 38 (5) (1998) 649.
[20] L. Marrelli et al., Proceedings of the 24th Conference on Controlled Fusion and Plasma Physics, 21A part I, Berchtesgaden, Germany, 1997, p. 333.
[21] L. Carraro et al., J. Nucl. Mater. 220–222 (1995) 646.